




Research Article

An Improved Power-Only Measurement Strategy for Calibrating Phased Array Antennas

Shuaizhao Li ^{1,2} Zhongjun Yu ^{1,2} Qiang Zhang,^{1,2} and Yunhua Luo ¹

¹Aerospace Information Research Institute, Chinese Academy of Sciences, Beijing 100190, China

²School of Electronic, Electrical and Communication Engineering University of Chinese Academy of Sciences, Beijing 100190, China

Correspondence should be addressed to Zhongjun Yu; yuzj@ucas.ac.cn

Received 11 May 2022; Accepted 15 July 2022; Published 12 August 2022

Academic Editor: Giacomo Oliveri

Copyright © 2022 Shuaizhao Li et al. This is an open access article distributed under the Creative Commons Attribution License, which permits unrestricted use, distribution, and reproduction in any medium, provided the original work is properly cited.

An improved power-only measurement method is proposed to calibrate phased arrays, which is aimed at solving two remaining problems: little contribution of one antenna element's phase shifting to the whole array's power and the ambiguity of solutions. The method includes four steps. Firstly, the random distributed phase of each element is adjusted to guarantee that it is -90° to $+90^\circ$ relative to the reference element. Secondly, the proper number of the elements shifting their phases together is approximately determined. Then, an invertible matrix is formed from the standard Hadamard matrix to split the array into different groups, which applies to an arbitrary number of elements; Finally, the array gets calibrated with an existing method. Numerical simulations and experiments are conducted to validate the effectiveness of the proposed method.

1. Introduction

Nowadays, phased arrays are playing a great role not only in military use [1], but also in emerging civil applications like the 5th Generation (5G) base station [2] and automotive radar of unmanned vehicle [3], attributing to their abilities of precise beamforming and flexible beam scanning [4, 5].

However, the initial excitation of each antenna channel of the phased array may vary with each other due to different signal path lengths, the characteristic fluctuation of components of each channel, temperature drift, and device ageing, which degrades the performance of the phased array. Besides the inaccurate channel excitations, also called calibration errors, mutual coupling between channels is another factor to be reckoned with. And a considerable amount of literature has been published on the effects of calibration errors and mutual coupling on the beam pattern. Schmid et al. [6] presented worst-case boundaries and a statistical analysis of the deviation of the beam pattern of an array in the presence of calibration errors and mutual coupling exploiting the Cauchy-Schwarz inequality. Based on the

interval analysis (IA) method [7], including Circular Interval Analysis (CIA) and Rectangular Interval Analysis (RIA), Anselmi et al. [8–13] conducted pattern sensitivity analysis of both linear arrays and reflector antennas. And Diao's research [14] indicated that mutual coupling increases antenna loss and deteriorates receiving efficiency. In addition, some researchers studied the effects of these errors on the accuracy of direction-of-arrival (DOA) estimation [15, 16].

Therefore, phased arrays must be calibrated before operation. Since phased arrays can work in transmitting mode or receiving mode and the calibration procedures for both of them are similar, we only explain the calibration methods in transmitting mode below.

There has been great work on calibrating phased arrays. A usual calibration method utilized in anechoic chambers is the near-field scanning probe method [17, 18], with which each channel is switched on and scatter parameters are measured when the probe scans exactly above the antenna element. This demands complex devices and accurate position systems and only applies to in-factory calibration. Another efficient calibration method is the phase-toggling

method [19, 20], with which several groups of proper phase settings for all elements are obtained and then the transmitted composite signal's amplitude and phase are measured. Some researchers utilize the mutual coupling effect [21–25] between antenna elements to calibrate phased arrays, whose structure tends to be symmetrical to some extent.

The calibration method we focus on is the rotating-element electric-field vector (REV) method because of its great potential at in higher frequencies for its power-only measurement scheme. The method was first proposed in 1982 by Mano [26]. Its principle is to shift one element's phase from 0° to 360° discretely depending on the applied phase shifter, with the phase of the other elements unchanged and the transmitted power of the whole array being measured each time. Finally, the amplitude and phase of the rotating element's initial excitation are calculated by a closed-form equation. However, the total number of measurements is quite huge and it consumes much time. In 2001, Sorace [27] proposed that it needs only 4 measurements to obtain one element's amplitude and phase utilizing a maximum likelihood algorithm, and the total number of measurements is reduced to $3N+1$ for an N -element phased array. In 2017, Long [28] pointed out that it is sufficient to go through 3 phase settings (0° , 90° , 180°) for the rotating element to obtain the amplitude and phase of its initial excitation. And the total number of measurements is reduced to $2N+1$. As far as we investigated within the existing improved versions based on the REV method, this is the calibration method with the minimum measurement number. In 2019, compared with Long's method, He [29] changed the 180° phase shifting condition to turn the rotating element off. And this method's measurement number is still $2N+1$.

Although Long's method reduces the measurement number immensely, there are still two problems remaining to be solved. The first is the little contribution of one antenna element's phase shifting to the whole array's power. Rotating one element's phase will not lead to a notable change in the received power of the receiving antenna especially for a large array. Thus, several elements shifting their phases together are expected. The second problem is the ambiguity of solutions. This is mainly caused by the uncertainty about whether the composite power of the rotating elements is smaller than that of the other elements. This problem is non-negligible with more rotating elements and a more discrete phase distribution among elements.

In this paper, we proposed an improved calibration method based on Long's method to solve the two problems mentioned above. And this applies to phased arrays with an arbitrary number of elements and a randomly distributed phase. The structure of this paper is summarized below. In Section 2, the theory of the improved calibration method is introduced in details. In Section 3, an 11-element microstrip antenna array is simulated and the improved method is applied. Then in Section 4, a practical array is used to conduct the calibration experiment in an anechoic chamber with a far-field setup. Finally, some conclusions are drawn in Section 5.

2. Methods

Figure 1 shows a typical far-field setup and signal model of the power-only calibration method. The transmitting signal $E_n e^{j\phi_n}$ ($n = 1, 2, \dots, N$) of each element is added together as a composite signal $E_0 e^{j\phi_0}$ according to the vector superposition principle, and then it is received by a receiving antenna to measure the composite signal's power. And we define $E_n^0 e^{j\phi_n^0}$ ($n = 1, 2, \dots, N$) as the excitation of the n th element. It should be noted that the transmitting signal of each element differs from each other even if all elements have the same excitation, mainly because of edge effect and mutual coupling. And what we actually calibrate with the REV-based method is $E_n e^{j\phi_n}$ ($n = 1, 2, \dots, N$), not $E_n^0 e^{j\phi_n^0}$ ($n = 1, 2, \dots, N$). Assuming that the m th element, called the rotating element, shifts its phase of Δ , the composite signal \vec{E} can be expressed by equation (1). And $E_{\bar{m}} e^{j\phi_{\bar{m}}}$ represents the vector sum of the transmitting signal of all elements except the rotating element.

$$\begin{aligned} \vec{E} &= (E_0 e^{j\phi_0} - E_m e^{j\phi_m}) + E_m e^{j(\phi_m + \Delta)} \\ &= E_{\bar{m}} e^{j\phi_{\bar{m}}} + E_m e^{j(\phi_m + \Delta)}. \end{aligned} \quad (1)$$

For Long's method, Δ has 3 states, which are separately 0 , 90° , and 180° . And the receiving power $P_0, P_{\pi/2}, P_\pi$ are calculated by the following equations

$$\begin{aligned} P_0 &= \left(E_{\bar{m}} e^{j\phi_{\bar{m}}} + E_m e^{j(\phi_m + 0)} \right) \left(E_{\bar{m}} e^{j\phi_{\bar{m}}} + E_m e^{j(\phi_m + 0)} \right)^* \\ &= (E_{\bar{m}}^2 + E_m^2) + E_{\bar{m}} E_m e^{j(\phi_{\bar{m}} - \phi_m)} + E_{\bar{m}} E_m e^{j(\phi_m - \phi_{\bar{m}})}. \end{aligned} \quad (2)$$

$$\begin{aligned} \frac{P_{\pi}}{2} &= \left(E_{\bar{m}} e^{j\phi_{\bar{m}}} + E_m e^{j\left(\phi_m + \frac{\pi}{2}\right)} \right) \\ &\quad \left(E_{\bar{m}} e^{j\phi_{\bar{m}}} + E_m e^{j\left(\phi_m + \frac{\pi}{2}\right)} \right)^* \\ &= (E_{\bar{m}}^2 + E_m^2) + E_{\bar{m}} E_m e^{j(\phi_{\bar{m}} - \phi_m)} \cdot e^{-\frac{j\pi}{2}} + E_{\bar{m}} E_m e^{j(\phi_m - \phi_{\bar{m}})} \cdot e^{\frac{j\pi}{2}}. \end{aligned} \quad (3)$$

$$\begin{aligned} P_\pi &= \left(E_{\bar{m}} e^{j\phi_{\bar{m}}} + E_m e^{j(\phi_m + \pi)} \right) \left(E_{\bar{m}} e^{j\phi_{\bar{m}}} + E_m e^{j(\phi_m + \pi)} \right)^* \\ &= (E_{\bar{m}}^2 + E_m^2) \\ &\quad + E_{\bar{m}} E_m e^{j(\phi_{\bar{m}} - \phi_m)} \cdot e^{-j\pi} + E_{\bar{m}} E_m e^{j(\phi_m - \phi_{\bar{m}})} \cdot e^{j\pi}. \end{aligned} \quad (4)$$

After solving the equations above, the closed-form solution of $E_m e^{j\phi_m} / (E_0 e^{j\phi_0})$ is given with Long's method. By changing m from 1 to N , the array gets calibrated.

However, there are two problems remaining to solve. The first is little contribution of one antenna element's phase shifting to the whole array's power. If E_m is too small, it leads

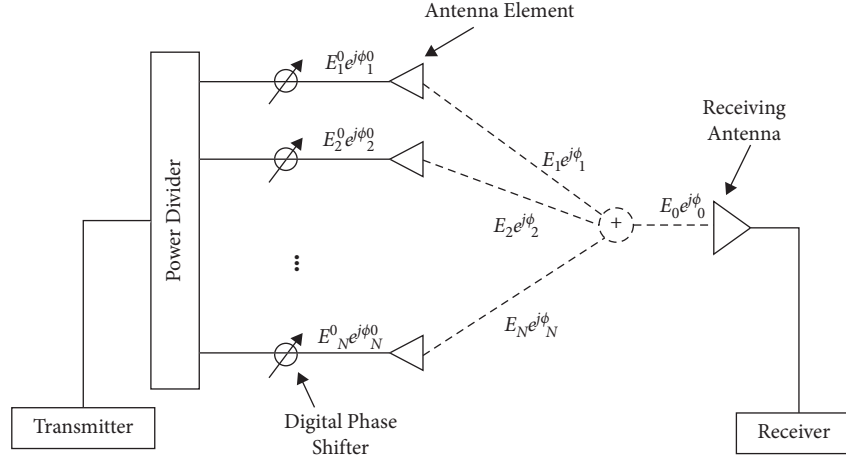


FIGURE 1: Far-field setup and signal model of the power-only calibration method.

to $P_0 \approx P_{\pi/2} \approx P_{\pi}$. In this case, the tiny difference among the three powers can hardly be detected, which results in an inaccurate solution of $E_m e^{j\phi_m} / (E_0 e^{j\phi_0})$. To solve this problem, enhancing the number of rotating elements is necessary. With several number of elements shifting their phase together, the composite power will see a significant change to be measured. Thus, a quite accurate solution of the ratio of the vector sum of the rotating elements' electrical field to the full array's composite field is obtained. It is a useful way to utilize Hadamard matrix to determine the exact rotating elements each time.

Mathematically, the order of a standard Hadamard matrix is 1, 2, or $4k$ ($k = 1, 2, \dots$). Here we construct an N -order matrix T_N :

$$T_N = \begin{bmatrix} H_{4k_1} & & & & & & \\ & H_{4k_2} & & & & & \\ & & \ddots & & & & \\ & & & & & & \\ & & & & H_{4k_p} & & \\ & & & & & & M_q \end{bmatrix}. \quad (5)$$

Here, $4k_1 + 4k_2 + \dots + 4k_p + q = N$, and H_{4k_n} ($n = 1, 2, \dots, p$) is a standard Hadamard matrix. To simplify T_N , the two conditions $4k_1 = 4k_2 = \dots = 4k_p = 4k_0$ and $0 \leq q < 4k_0$ are fulfilled.

As is known, the standard Hadamard matrix consists of two elements: 1 and -1 . And it is a positive definite matrix. To make H_{4k_0} only contain elements 1, 0 and make the number of the element 1 of every row equal, the following elementary transformation including two steps is carried out.

Step 1. Each row of the matrix except the first row is added by the first row and then divided by 2.

$$H_4 = \begin{bmatrix} 1 & 1 & 1 & 1 \\ 1 & -1 & 1 & -1 \\ 1 & 1 & -1 & -1 \\ 1 & -1 & -1 & 1 \end{bmatrix} \Rightarrow \begin{bmatrix} 1 & 1 & 1 & 1 \\ 1 & 0 & 1 & 0 \\ 1 & 1 & 0 & 0 \\ 1 & 0 & 0 & 1 \end{bmatrix} \Rightarrow R_4 = \begin{bmatrix} 0 & 1 & 0 & 1 \\ 1 & 0 & 1 & 0 \\ 1 & 1 & 0 & 0 \\ 1 & 0 & 0 & 1 \end{bmatrix}$$

FIGURE 2: An example of standard Hadamard matrix H_{4k_0} transforming into R_{4k_0} .

Step 2. The first row of the matrix subtracts the second row.

It should be noted that the elementary transformation will not change the invertibility of the matrix. Thus, the transformed matrix H_{4k_0} , renamed as R_{4k_0} , is an invertible matrix. Here is an example showed in Figure 2 to explain the procedure in detail.

The q -order principal minor sequence of H_{4k_0} is set as M_q . Mathematically, the principal minor sequence of a positive definite matrix is an invertible matrix. Thus, M_q is an invertible matrix. Then it is transformed with the two steps above. And the transformed matrix, renamed as R_q , is also an invertible matrix. Here is an example showed in Figure 3.

Finally, we construct an N -order invertible matrix R_N . And it is used for group dividing. The element 1 in every row represents the rotating elements for every measurement and the number of the rotating elements is $2k_0$, which is an even number, except the rotating elements included in matrix R_q .

$$R_N = \begin{bmatrix} R_{4k_0} & & & & \\ & R_{4k_0} & & & \\ & & \ddots & & \\ & & & & R_{4k_0} \\ & & & & & R_q \end{bmatrix} \quad (6)$$

$$H_4 = \begin{bmatrix} 1 & 1 & 1 & 1 \\ 1 & -1 & 1 & -1 \\ 1 & 1 & -1 & -1 \\ 1 & -1 & -1 & 1 \end{bmatrix} \rightarrow M_3 = \begin{bmatrix} 1 & 1 & 1 \\ 1 & -1 & 1 \\ 1 & 1 & -1 \end{bmatrix} \rightarrow R_3 = \begin{bmatrix} 0 & 1 & 0 \\ 1 & 0 & 1 \\ 1 & 1 & 0 \end{bmatrix}$$

FIGURE 3: An example of standard Hadamard matrix H_{4k_0} transforming into R_q ($0 < q < 4k_0$).

For every measurement, the ratio $Y_n e^{j\beta_n}$ ($n = 1, 2, \dots, N$) of the composite field of the rotating elements to the full array's composite field is obtained by Long's method. Thus,

$$R_N \cdot \begin{bmatrix} \frac{(E_1 e^{j\phi_1})}{(E_0 e^{j\phi_0})} \\ \frac{(E_2 e^{j\phi_2})}{(E_0 e^{j\phi_0})} \\ \vdots \\ \frac{(E_N e^{j\phi_N})}{(E_0 e^{j\phi_0})} \end{bmatrix} = \begin{bmatrix} Y_1 e^{j\beta_1} \\ Y_2 e^{j\beta_2} \\ \vdots \\ Y_N e^{j\beta_N} \end{bmatrix}. \quad (7)$$

So $E_n e^{j\phi_n} / (E_0 e^{j\phi_0})$ ($n = 1, 2, \dots, N$) can be figured out with the following equation

$$\begin{bmatrix} \frac{(E_1 e^{j\phi_1})}{(E_0 e^{j\phi_0})} \\ \frac{(E_2 e^{j\phi_2})}{(E_0 e^{j\phi_0})} \\ \vdots \\ \frac{(E_N e^{j\phi_N})}{(E_0 e^{j\phi_0})} \end{bmatrix} = R_N^{-1} \cdot \begin{bmatrix} Y_1 e^{j\beta_1} \\ Y_2 e^{j\beta_2} \\ \vdots \\ Y_N e^{j\beta_N} \end{bmatrix}. \quad (8)$$

The second problem is ambiguity of solutions. This is mainly caused by the uncertainty whether the composite power of the rotating elements is smaller than that of the other elements. The solution is to figure out a proper number of rotating elements to ensure that the composite power of the rotating elements is smaller. However, if the distributed phases of all elements are too discrete, there is still a little possibility that the composite power of the rotating elements is bigger even if there is only one rotating element. Thus, first of all, the phases range of all elements should be narrowed. Choosing the first element as reference element, the composite field of the first element and the n th element is expressed as follows:

$$\vec{E}_{1n} = E_1 e^{j\phi_1} + E_n e^{j\phi_n} = e^{j\phi_1} (E_1 + E_n e^{j(\phi_n - \phi_1)}). \quad (9)$$

And its power can be expressed as follows:

$$P_{1n} = E_1^2 + E_n^2 + 2E_1 E_n \cos(\phi_n - \phi_1). \quad (10)$$

Reversing the phase of the n th element, the composite field and its power change as follows:

$$\vec{E}_{1n}^r = E_1 e^{j\phi_1} + E_n e^{j(\phi_n + \pi)} = e^{j\phi_1} (E_1 - E_n e^{j(\phi_n - \phi_1)}), \quad (11)$$

$$P_{1n}^r = E_1^2 + E_n^2 - 2E_1 E_n \cos(\phi_n - \phi_1).$$

If $|\phi_n - \phi_1| \leq \pi/2$, $P_{1n} \geq P_{1n}^r$, which means that the composite power of the first element and the n th element decreases after reversing the phase of the n th element. And if $\pi/2 < |\phi_n - \phi_1| \leq \pi$, the composite power increases after reversing the phase of the n th element. Utilizing this effect, here are three steps to limit the phases of all elements within $[-90^\circ, +90^\circ]$:

- (i) Step 1: choosing the first element as the reference element, switch on the first element with the other elements terminated.
- (ii) Step 2: switch on the second element and measure the far-field composite power. Then reverse the phase of the second element and measure the composite power. If the power decreases, reverse the phase of the second element again to recover. And if the power increases, keep the phase of the second element unchanged. Finally, switch off the second element.
- (iii) Step 3: carry out the same procedure as step 2 for the other elements. Finally, switch off the first element.

After adjusting the phases of all elements within $[-90^\circ, +90^\circ]$ relative to the reference element, the proper number of the rotating elements should be figured out. The number should be sufficiently big to ensure that the phase change of the rotating elements contributes much to the power of the whole array. However, lots of rotating elements will not promise that the composite power of the rotating elements is smaller than that of the other elements. Here, we separately define t_1 as the ratio of the composite power of the rotating elements to that of the whole array and define t_2 as the ratio of the composite power of the rotating elements to that of the other elements.

$$t_1 = \frac{|\sum_{n=1}^M E_n e^{j\phi_n}|^2}{|\sum_{n=1}^N E_n e^{j\phi_n}|^2}. \quad (12)$$

$$t_2 = \frac{|\sum_{n=1}^M E_n e^{j\phi_n}|^2}{|\sum_{n=1}^N E_n e^{j\phi_n} - \sum_{n=1}^M E_n e^{j\phi_n}|^2}, \quad (13)$$

where M is the number of the rotating elements. We should ensure $10 \lg(t_1) > \delta$ and $t_2 < 1$, where δ is a parameter relative to the sensitivity of the measurement device. And it is a useful way to utilize Monte Carlo method to figure out the

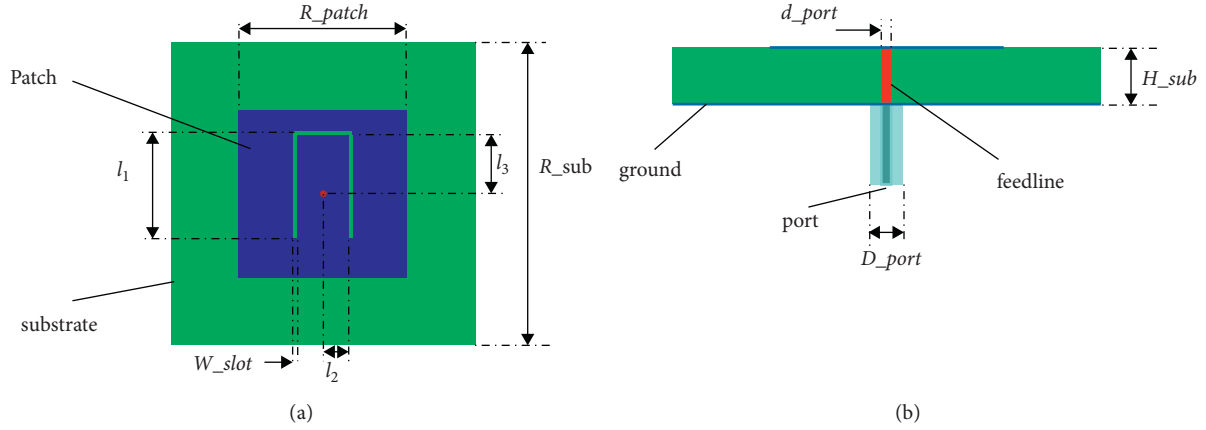


FIGURE 4: (a) The top view and (b) the front view of the patch antenna.

TABLE 1: The parameters of the patch antenna.

Parameters	R_{sub}	H_{sub}	R_{patch}	W_{slot}	l_1	l_2	l_3	D_{port}	d_{port}
Value (mm)	16	2.1	8.8	0.2	5.66	1.36	3.1	1.3	0.38

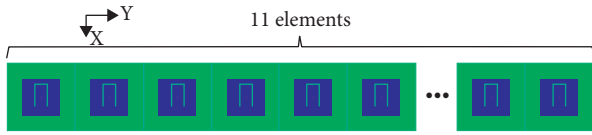


FIGURE 5: The arrangement of the 11-element ULA.

proper M to make the probability of the two events $10\lg(t_1) > \delta$ and $t_2 < 1$ close to 1.

3. Numerical Simulations

To validate the effectiveness of the improved calibration method based on Long's method, a microstrip patch antenna operating at 9.5 GHz is studied. Its structure and parameters are separately described by Figure 4 and Table 1. And the material of the substrate is Rogers 5880. A uniform linear array (ULA) described by Figure 5 consisting of 11 antenna elements, simulated by high-frequency structure simulator (HFSS), is the object we apply the method to. Numbering the elements from left to right, the amplitudes E_n^0 ($n = 1, 2, \dots, 11$) and phases ϕ_n^0 ($n = 1, 2, \dots, 11$) of excitations of allelements are set to follow uniform distribution, separately $E_n^0 \sim U(-1.5 \text{ dB}, +1.5 \text{ dB})$ and $\phi_n^0 \sim U(-180^\circ, +180^\circ)$. Here are two sets of data used as the initial distribution of the excitations of all elements, shown in Table 2. The detailed calibration procedures mainly include 4 steps.

Step 1: limit the phase distribution within $[-90^\circ, +90^\circ]$

Firstly, select the first element as the reference element and maintain its excitation. And for the other elements, replace their amplitudes with 0 as a state 'off'. Then for the second element, replace its amplitude 0 with its initial amplitude -0.45 dB as a state 'on' and record the far-field realized gain at boresight. Later with the phase of the second element adding 180° , record the gain

value again and then change its state into 'off'. And for the n th ($n = 3, 4, \dots, 11$) elements, carry out the same procedure. In short, each time there are only the first element and the n th ($n = 2, 3, 4, \dots, 11$) element working, and the realized gain of them separately with their initial phases unchanged and with the n th element reversing its phase are recorded, as Figure 6 shows.

Finally, according to our theory mentioned in Section 2, since the realized gain decreases with the p th ($p = 2, 4, 5, 10, 11$) element reversing their phases, we reverse their phases again to recover. And Table 3 records the excitations of all elements after adjustment and the phase distribution now is within $[-90^\circ, +90^\circ]$.

Step 2: figure out the proper number of rotating elements

For (12) and (13), set $N = 11$ and make E_n ($n = 1, 2, \dots, 11$) and ϕ_n ($n = 1, 2, \dots, 11$) follow uniform distribution, separately $E_n \sim U(-1.5 \text{ dB}, +1.5 \text{ dB})$ and $\phi_n \sim U(-180^\circ, +180^\circ)$. Our target is to figure out the proper M to make the probability of the two events $10\lg(t_1) > \delta$ and $t_2 < 1$ close to 1. Thus, for each possible value of M , a group of Monte Carlo tests are simulated to calculate the probability of the two events. And for each group of Monte Carlo tests, only E_n and ϕ_n are varied. Here we set the number of tests as 10000 for each group. We define P_1 as the probability of event1: $10\lg(t_1) > \delta$ and P_2 as the probability of event2: $t_2 < 1$. Since one of our targets is to make P_2 close to 1, the condition $M \leq \lfloor N/2 \rfloor$ should be fulfilled, which means that the number of rotating elements is no more than half of the total number of elements. And Figure 7 demonstrates how P_1 and P_2 change while M varies.

As seen from Figure 7, with the number of rotating elements getting bigger, P_1 increases and P_2 decreases.

TABLE 2: The initial excitations of all elements.

Element number	1	2	3	4	5	6	7	8	9	10	11
Amplitude (dB)	0	-0.45	1.32	1.13	0.15	0.37	0.26	-0.88	-0.6	-0.09	-0.81
Phase (°)	0	67	-114	-47	45	101	-151	155	99	-5	-23

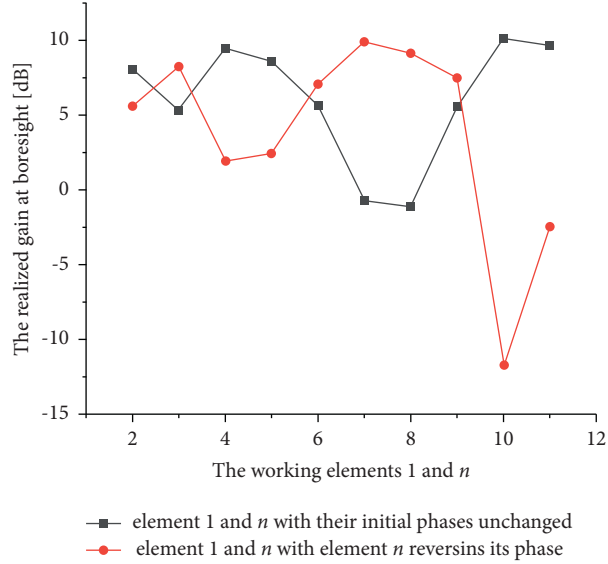


FIGURE 6: The realized gain of element 1 and element (n).

TABLE 3: The excitations of all elements after adjustment.

Element number	1	2	3	4	5	6	7	8	9	10	11
Amplitude (dB)	0	-0.45	1.32	1.13	0.15	0.37	0.26	-0.88	-0.6	-0.09	-0.81
Phase (°)	0	67	66	-47	45	-79	29	-25	-81	-5	-23

And with the sensitivity of the measurement device getting higher while M maintains, P_1 increases, which means that it is much easier to detect the power change of the whole array when the phases of some elements change. Set $\delta = -30$ dB and the target of making P_1 and P_2 close to 1 can be fulfilled when $M = 1, 2$ or 3 . And we choose the even number, which is 2 rotating elements.

Step 3: create group dividing matrix

Making $2k_0 = 2$, thus the order of the standard Hadamard matrix utilized is $4k_0 = 4$. And the group dividing matrix R_{11} can be expressed as follows:

$$R_{11} = \begin{bmatrix} R_4 & & \\ & R_4 & \\ & & R_3 \end{bmatrix} \quad (14)$$

where $R_4 = \begin{bmatrix} 0 & 1 & 0 & 1 \\ 1 & 0 & 1 & 0 \\ 1 & 1 & 0 & 0 \\ 1 & 0 & 0 & 1 \end{bmatrix}$, $R_3 = \begin{bmatrix} 0 & 1 & 0 \\ 1 & 0 & 1 \\ 1 & 1 & 0 \end{bmatrix}$. And the ele-

ment 1 in every row in matrix R_{11} represents the rotating element each time.

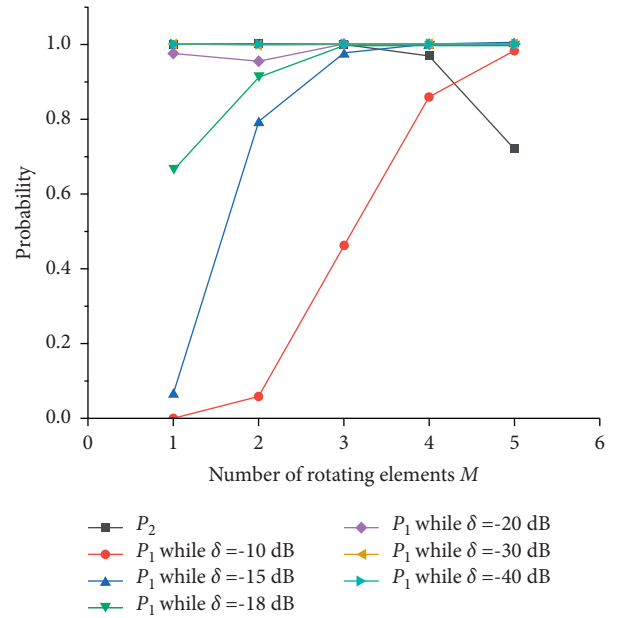
FIGURE 7: The probability of event1 and event2 while (M) varies.

TABLE 4: The realized gains with the phases of rotating elements changing separately 90° and 180°.

Group	1	2	3	4	5	6	7	8	9	10	11
Rotate 90°(dB)	11.21	8.41	9.10	12.01	13.31	8.21	11.99	10.36	11.46	13.13	12.57
Rotate 180°(dB)	9.33	8.62	8.69	6.51	11.02	9.05	10.58	8.83	9.60	10.56	9.57

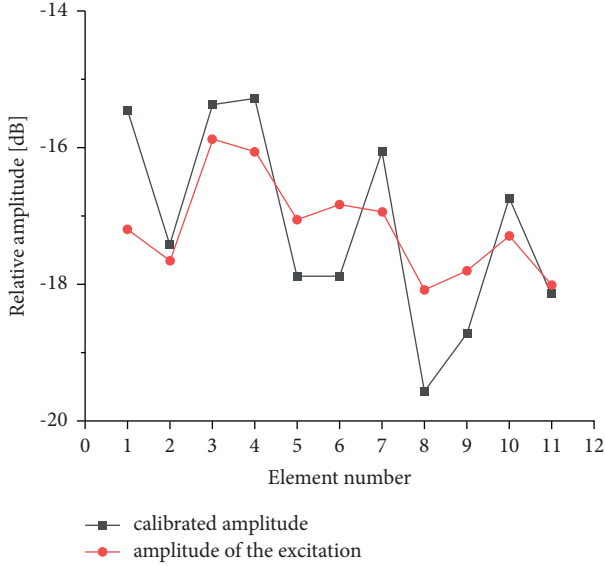


FIGURE 8: Relative amplitude comparison between calibrated result and excitation.

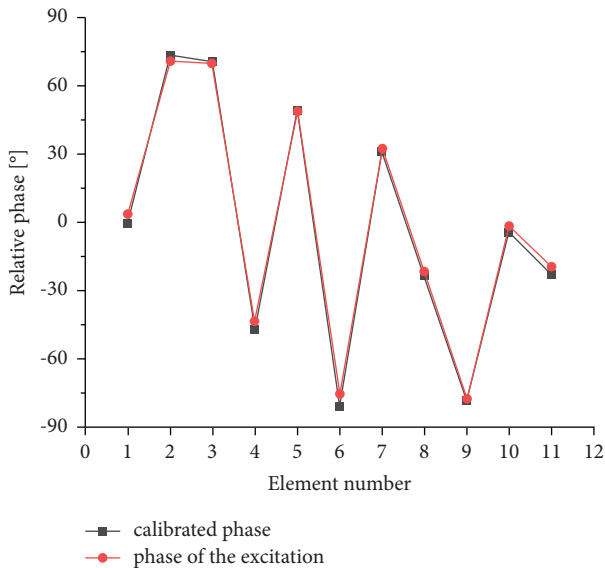


FIGURE 9: Relative phase comparison between calibrated result and excitation.

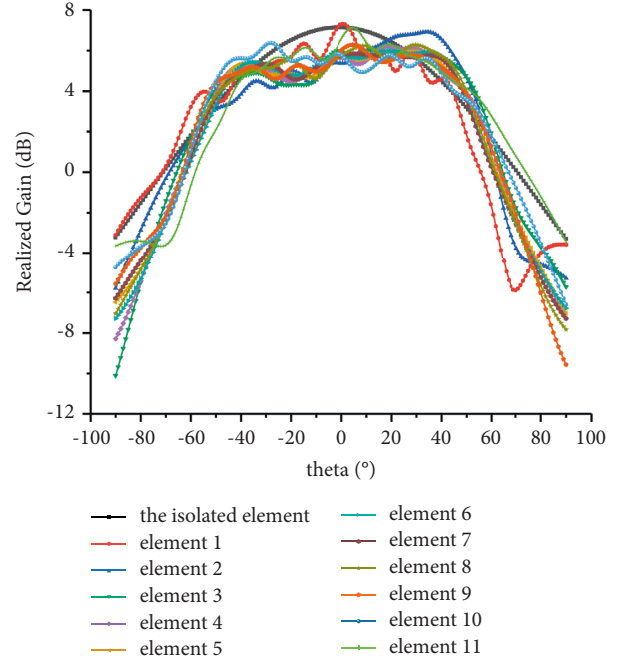


FIGURE 10: The active element patterns of all elements.

Step 4: calibrate with Long’s method

According to Long’s method, the realized gain of the whole array at boresight with excitations after adjustment in Step 1 is recorded, which is 12.57 dB. Then for each group including rotating elements and the other unchanged elements, the realized gains with the phases of rotating elements changing separately 90° and 180° are recorded, shown in Table 4. And the total number of measurements is $2N + 1 = 23$.

With Long’s method and (8), $E_n e^{j\phi_n} / (E_0 e^{j\phi_0})$ ($n = 1, 2, \dots, 11$) are finally calculated, which are compared with $E_n^0 e^{j\phi_n^0} / \sum_{n=1}^{11} E_n^0 e^{j\phi_n^0}$ ($n = 1, 2, \dots, 11$), shown in Figure 8 and 9.

As seen from Figures 8 and 9, the calibrated result is close to the elements’ excitation in the aspect of phase but quite different from that in terms of amplitude. This is because the transmitting signal of each element differs from each other even if all elements have the same excitation mainly due to

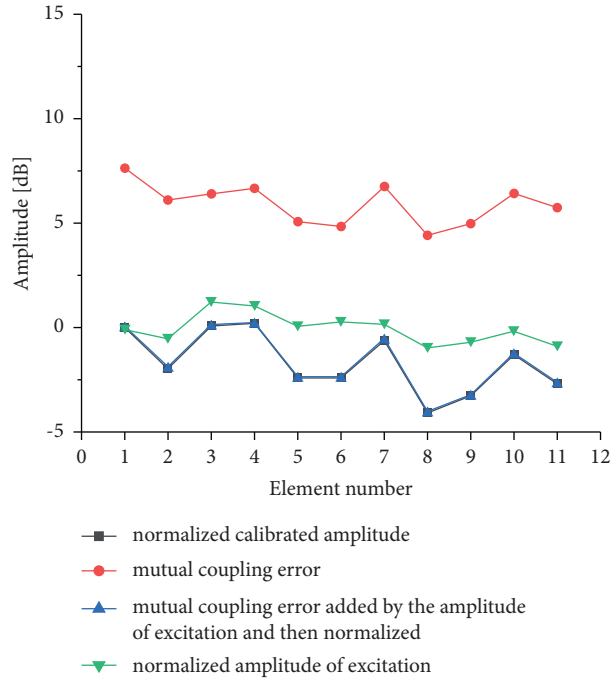


FIGURE 11: Normalized calibrated amplitude result in the presence of mutual coupling error.

edge effect and mutual coupling. Figure 10 shows the active element patterns of all elements.

The realized gains of the active patterns of all elements at boresight are recorded. And they are regarded as mutual coupling error. After added by the amplitudes of the excitations and normalized to the first element, they are compared to the normalized amplitudes of the calibrated result, shown in Figure 11.

As seen from Figure 11, the normalized calibrated amplitude is with good accordance to the normalized sum of the mutual coupling error and the amplitude of excitation. And the detailed calibration root-mean-square error is separately 0.01 dB in terms of amplitude, and 2.91° in terms of phase calculated from Figure 9. Thus, the numerical simulation experiment validates the effectiveness and accuracy of the improved calibration method. Especially, this method calibrates not only excitation error but also mutual coupling error.

4. Experiments

To verify the practicability of our improved calibration method, a two-dimension phased array operating at 9.5 GHz is utilized for the calibration experiment, shown in Figure 12. Only 11 elements shown in Figure 13 are selected to conduct the experiment for time saving. And the setup of the experiment is in a far-field anechoic chamber, shown in Figure 14. The array works in receiving mode and a horn antenna connected to a signal generator transmits signal. And a spectrum analyzer connected to the array is used to measure the composite power of the 11 elements.

The 11 elements are with unknown random distributed amplitudes and phases. And the calibration procedures are similar to the process in Section 3. After calibrating the amplitudes and phases of the 11 elements with our improved

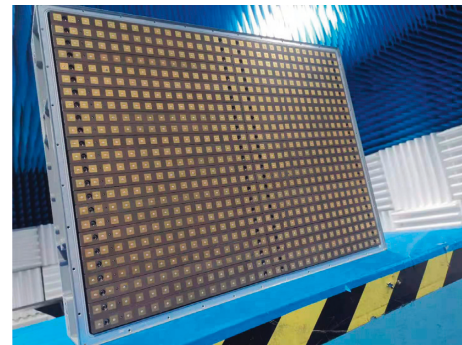


FIGURE 12: The two-dimension phased array utilized for experiment.

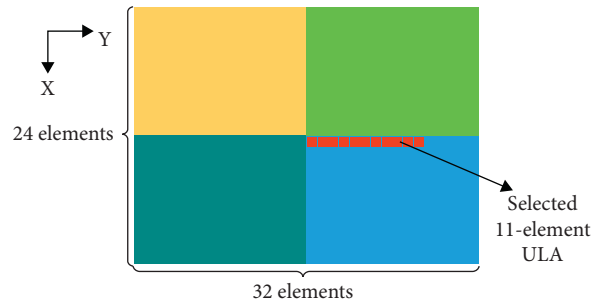


FIGURE 13: Specially selected 11 elements for experiment.

method, the radiation patterns of the 11 elements before and after calibration are separately measured, shown in Figure 15. And the radiation pattern after calibration shows good characteristic with approximately -13 dB side lobe. Thus, the practicability of our method gets verified.

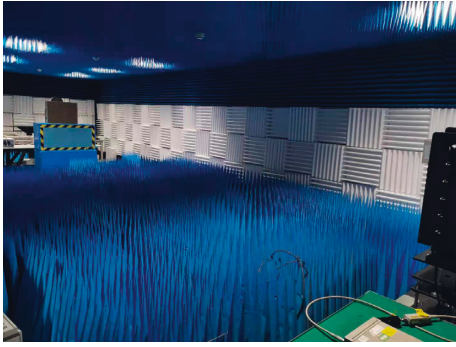


FIGURE 14: The far-field setup of the experiment.

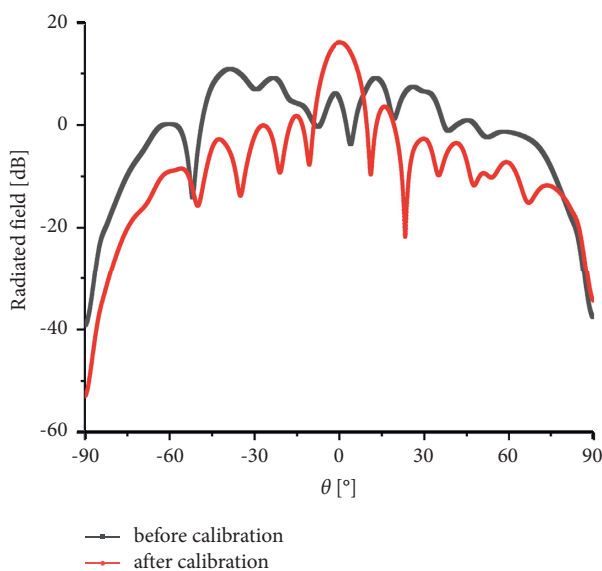


FIGURE 15: The radiation patterns of the 11 elements before and after calibration.

5. Conclusion

This paper proposed an improved power-only method for phased array calibration. When there are lots of elements, only one rotating element shifting its phase won't contribute much to the power of the whole array. And our method gives a scientific way to figure out the proper number of rotating elements and create an invertible matrix for group dividing. This method also applies to phased arrays with random distributed phases, which easily cause ambiguity of solutions. The numerical simulations validate the calibration accuracy of our method and the experiments utilizing practical phased array verify the effectiveness of our method.

Data Availability

The data used to support the findings of this study are available from the corresponding author on reasonable request.

Conflicts of Interest

The authors declare that there are no conflicts of interest regarding the publication of this paper.

References

- [1] J. C. Rock, J. H. Mullins, J. P. Booth, and T. Hudson, "The Past, Present, and Future of Electronically-Steerable Phased Arrays in Defense Applications," in *Proceedings of the 2008 IEEE Aerospace Conference*, pp. 1–7, Big Sky, MT, USA, March 2008.
- [2] R. Flamini, C. Mazzucco, R. Lombardi, C. Massagrande, F. Morgia, and A. Milani, "Millimeter-wave phased arrays for 5G: an industry view on current issues and challenges," in *Proceedings of the 2019 IEEE International Symposium on Phased Array System & Technology (PAST)*, pp. 1–2, Waltham MA USA, October 2019.
- [3] U. Chipengo, P. M. Krenz, and S. Carpenter, "From antenna design to high fidelity, full physics automotive radar sensor corner case simulation," *Modelling and Simulation in Engineering*, Article ID 4239725, 2018.
- [4] C. A. Balanis, *Antenna Theory: Analysis and Design*, Wiley, Hoboken, 2016.
- [5] R. J. Mailloux, *Phased Array Antenna Handbook*, Artech House, Norwood, 2017.
- [6] C. M. Schmid, S. Schuster, R. Feger, and A. Stelzer, "On the effects of calibration errors and mutual coupling on the beam pattern of an antenna array," *IEEE Transactions on Antennas and Propagation*, vol. 61, no. 8, pp. 4063–4072, 2013.
- [7] R. E. Moore, *Interval Analysis*, Prentice-Hall, Englewood Cliffs, NJ, USA, 1966.
- [8] N. Anselmi, M. Salucci, P. Rocca, and A. Massa, "Power pattern sensitivity to calibration errors and mutual coupling in linear arrays through circular interval arithmetics," *Sensors*, vol. 16, no. 6, p. 791, 2016.
- [9] N. Anselmi, L. Manica, P. Rocca, and A. Massa, "Tolerance analysis of antenna arrays through interval arithmetic," *IEEE Transactions on Antennas and Propagation*, vol. 61, no. 11, pp. 5496–5507, 2013.
- [10] P. Rocca, L. Manica, N. Anselmi, and A. Massa, "Analysis of the pattern tolerances in linear arrays with arbitrary amplitude errors," *IEEE Antennas and Wireless Propagation Letters*, vol. 12, pp. 639–642, 2013.
- [11] L. Poli, P. Rocca, N. Anselmi, and A. Massa, "Dealing with uncertainties on phase weighting of linear antenna arrays by means of interval-based tolerance analysis," *IEEE Transactions on Antennas and Propagation*, vol. 63, no. 7, pp. 3229–3234, 2015.
- [12] P. Rocca, N. Anselmi, and A. Massa, "Interval arithmetic for pattern tolerance analysis of parabolic reflectors," *IEEE Transactions on Antennas and Propagation*, vol. 62, no. 10, pp. 4952–4960, 2014.
- [13] P. Rocca, L. Manica, and A. Massa, "Interval-based analysis of pattern distortions in reflector antennas with bump-like surface deformations," *IET Microwaves, Antennas & Propagation*, vol. 8, no. 15, pp. 1277–1285, 2014.
- [14] J. Diao and K. F. Warnick, "Antenna loss and receiving efficiency for mutually coupled arrays," *IEEE Transactions on Antennas and Propagation*, vol. 65, no. 11, pp. 5871–5877, 2017.
- [15] A. L. Swindlehurst and T. Kailath, "A performance analysis of subspace-based methods in the presence of model errors.

- I. The MUSIC algorithm,” *IEEE Transactions on Signal Processing*, vol. 40, no. 7, pp. 1758–1774, 1992.
- [16] H. Chen, X. Li, W. Jiang, and Z. Zhuang, “MIMO radar sensitivity analysis of antenna position for direction finding,” *IEEE Transactions on Signal Processing*, vol. 60, no. 10, pp. 5201–5216, 2012.
- [17] M. Scott, “SAMPSON MFR active phased array antenna,” *IEEE International Symposium on Phased Array Systems and Technology*, pp. 119–123, 2003.
- [18] M. Sarcione, J. Mulcahey, D. Schmidt et al., “The design, development and testing of the THAAD (Theater High Altitude Area Defense) solid state phased array (formerly ground based radar),” in *Proceedings of International Symposium on Phased Array Systems and Technology*, pp. 260–265, Boston, MA, USA, October 1996.
- [19] K.-M. Lee, R.-S. Chu, and S.-C. Liu, “A built-in performance-monitoring/fault isolation and correction (PM/FIC) system for active phased-array antennas,” *IEEE Transactions on Antennas and Propagation*, vol. 41, no. 11, pp. 1530–1540, 1993.
- [20] R. Long, J. Ouyang, F. Yang, W. Han, and L. Zhou, “Multi-element phased array calibration method by solving linear equations,” *IEEE Transactions on Antennas and Propagation*, vol. 65, no. 6, pp. 2931–2939, 2017.
- [21] H. M. Aumann, A. J. Fenn, and F. G. Willwerth, “Phased array antenna calibration and pattern prediction using mutual coupling measurements,” *IEEE Transactions on Antennas and Propagation*, vol. 37, no. 7, pp. 844–850, 1989.
- [22] A. Nafe, K. Kibaroglu, M. Sayginer, and G. M. Rebeiz, “An In-Situ Self-Test and Self-Calibration Technique Utilizing Antenna Mutual Coupling for 5G Multi-Beam TRX Phased Arrays,” in *Proceedings of the 2019 IEEE MTT-S International Microwave Symposium (IMS)*, pp. 1229–1232, Boston, MA, USA, July 2019.
- [23] C. Shipley and D. Woods, “Mutual coupling-based calibration of phased array antennas,” *Proceedings 2000 IEEE International Conference on Phased Array Systems and Technology*, pp. 529–532, 2000.
- [24] R. M. Lebrón, P. S. Tsai, J. M. Emmett, C. Fulton, and J. L. Salazar-Cerreno, “Validation and testing of initial and in-situ mutual coupling-based calibration of a dual-polarized active phased array antenna,” *IEEE Access*, vol. 8, pp. 78315–78329, 2020.
- [25] Y. Neidman, R. Shavit, and A. Bronshtein, “Diagnostic of phased arrays with fault elements using the mutual coupling method,” in *Proceedings of the 2008 IEEE International Conference on Microwaves, Communications, Antennas and Electronic Systems*, pp. 1–6, Tel-Aviv, Israel, May 2008.
- [26] S. Mano and T. Katagi, “A method for measuring amplitude and phase of each radiating element of a phased array antenna,” *Electronics and Communications in Japan*, vol. 65, no. 5, pp. 58–64, 1982.
- [27] R. Sorace, “Phased array calibration,” *IEEE Transactions on Antennas and Propagation*, vol. 49, no. 4, pp. 517–525, 2001.
- [28] R. Long, J. Ouyang, F. Yang, W. Han, and L. Zhou, “Fast amplitude-only measurement method for phased array calibration,” *IEEE Transactions on Antennas and Propagation*, vol. 65, no. 4, pp. 1815–1822, 2017.
- [29] G. He, X. Gao, and H. Zhou, “Fast phased array calibration by power-only measurements twice for each antenna element,” *International Journal of Antennas and Propagation*, pp. 1–10, Article ID 6432149, 2019.